Graphene-on-Paper Sound Source Devices

He Tian,[†,‡] Tian-Ling Ren,[†,‡,*] Dan Xie,[†,‡] Yu-Feng Wang,[†,‡] Chang-Jian Zhou,[†,‡] Ting-Ting Feng,[†,‡] Di Fu,[†,‡] Yi Yang,[†,‡] Ping-Gang Peng,[†,‡] Li-Gang Wang,[†,‡] and Li-Tian Liu[†,‡]

[†]Institute of Microelectronics, Tsinghua University, Beijing 100084, China and [‡]Tsinghua National Laboratory for Information Science and Technology (TNList), Tsinghua University, Beijing 100084, China

ABSTRACT We demonstrate an interesting phenomenon that graphene can emit sound. The application of graphene can be expanded in the acoustic field. Graphene-on-paper sound source devices are made by patterning graphene on paper substrates. Three graphene sheet samples with the thickness of 100, 60, and 20 nm were fabricated. Sound emission from graphene is measured as a function of power, distance, angle, and frequency in the far-field. The theoretical model of air/graphene/paper/PCB board multilayer structure is established to analyze the sound directivity, frequency response, and efficiency. Measured sound pressure level (SPL) and efficiency are in good agreement with theoretical results. It is found that graphene has a significant flat frequency response in the wide ultrasound range 20−50 kHz. In addition, the thinner graphene sheets can produce higher SPL due to its lower heat capacity per unit area (HCPUA). The infrared thermal images reveal that a thermoacoustic effect is the working principle. We find that the sound performance mainly depends on the HCPUA of the conductor and the thermal properties of the substrate. The paper-based graphene sound source devices have highly reliable, flexible, no mechanical vibration, simple structure and high performance characteristics. It could open wide applications in multimedia, consumer electronics, biological, medical, and many other areas.

KEYWORDS: graphene · sound souce · paper-based · thermoacoutic effect · acoustic characterization · frequency response

Graphene, a novel material first found in 2004,[1] has attracted much research interest due to its excellent structural and electrical properties. It has a huge electrical mobility approaching 200000 $cm^2 V^{-1} s^{-1}$ for a free sheet for both electrons and holes.[2,3] Moreover, the thermal conductivity of suspended graphene is ~5000 $W m^{-1} K^{-1}$ which is the highest compared with that of other materials.[4] With its extraordinary properties, graphene has many uses in electronic, mechanical, photonic and thermal applications. Many kinds of graphene-based devices have been fabricated such as field effect transistor,[5] nonvolatile memory,[6] resonator,[7] transparent electrode,[8] photodetector,[9] gas sensor,[10] and heat spreader.[11−13] However an acoustic application for graphene has not been reported.

In this paper, an interesting phenomenon that graphene can emit sound was studied. Our novel paper-based graphene sound source devices were fabricated by a simple process. In comparison with a silicon-based standard technique, paper-based systems can open a new venue of technologies.[14−16] Paper is chosen as a substrate due to its superior quality. It is lightweight, low cost, readily available, and easy to manufacture. Particularly, it has low thermal conductivity which can be used as an ideal insulating substrate. Graphene is used as a sound emission component due to its ultrasmall heat capacity per unit area (HCPUA). The combination of exceptional electrical transport and thermal properties suggests that novel nanometer-thickness thermophones[17−27] are different from conventional arrangements.

RESULTS AND DISCUSSION

Figure 1a shows a schematic diagram of a graphene-on-paper sound source device. In this structure, a graphene film is located at the center of the paper. When sound frequency electric signal is applied to graphene through the silver contact, the joule heating will heat up the air near its surface, then the periodicity of air vibration will form sound waves. Figure 1b summarizes the process used in fabricating the device.

The photograph of a paper-based graphene sound source is shown in Figure 1c. The 30−50 μm apertures filter paper is used as the substrate. The conductive silver ink is used as electrode. Figure 1d shows the scanning electron microscope (SEM) image of the graphene. Some ripples of graphene can be seen clearly. Figure 1e shows the optical photograph of graphene after oxygen plasma etching (OPE). Figure 1f shows the Raman spectra (514.5 nm laser wavelength) obtained from the corresponding colored spots in Figure 1e. Two prominent peaks appear at 1582 and 2700 cm^{-1}, corresponding to G and 2D bands, respectively. The film exhibits typical multilayered graphene (MLG) characteristics

* Address correspondence to RenTL@tsinghua.edu.cn.

Received for review March 13, 2011 and accepted May 19, 2011.

Published online May 19, 2011
10.1021/nn2009535

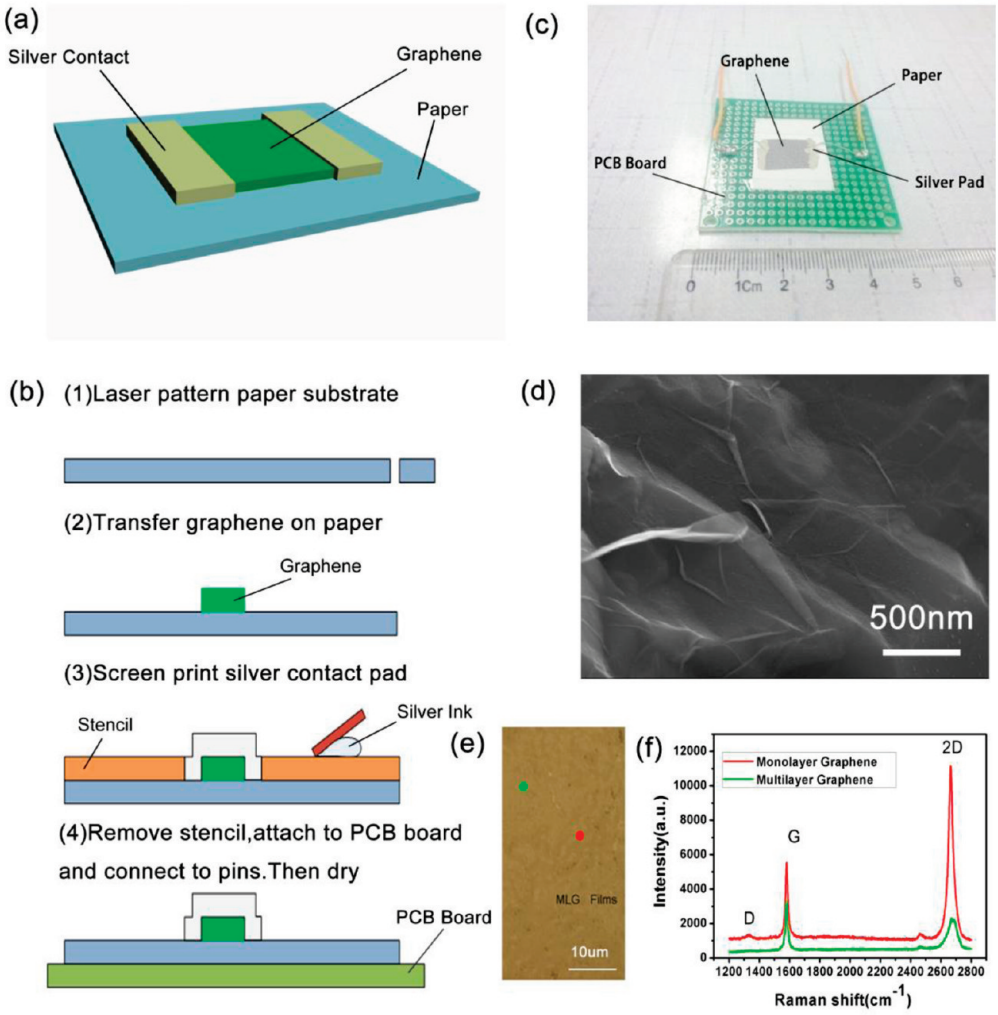

Figure 1. Graphene-on-paper sound source devices. (a) Schematic view of a paper-based sound source device using graphene as the emission component. (b) Fabrication process of the paper-based graphene sound source device. (c) Photograph of a graphene/paper sound source device with a 1 cm^2 emission area. (d) SEM image of graphene. (e) An optical image of the graphene after oxygen plasma etching. (f) Raman spectrum in the range of 1200−2800 cm^{-1} of the graphene. The red line and green line correspond to the red and green part in Figure 1e, respectively.

with a strong G peak and a broad 2D peak (green line), while some spots exhibit monolayer graphene feature with a sharp G peak and a single 2D peak with higher intensity (red line). The small intensity of D-band observed at 1350 cm^{-1} indicates the low levels of defects and local-disorders in the deposited films. The X-ray diffraction (XRD) cure of MLG is available in Supporting Information (Figure S2). As the peak intensity of the (002) diffraction line is at 26.48°, it illustrates the interlayer distance is 0.336 nm. The typical feature of the graphite peak at (001) is not identified in this graphene XRD pattern, which indicates MLG is not composed of conventional thin graphite sheets.[28,29]

Three samples of paper-based graphene sound source devices are measured, named sample 1, sample 2, and sample 3. The resistance of the three samples are 32, 143, and 601 Ω, respectively. The area of the graphene is about 1 × 1 cm^2, and the average thickness of three graphene sheet samples are about 100, 60, and 20 nm, respectively. The test platform contains a signal generator, a standard microphone, and a dynamic signal analyzer as shown in Figure 2a. The graphene sound source is directly tested by using a standard microphone (Figure 2b). The distance from the sound source to the microphone is 5 cm.

The output sound pressure (SP) of the paper-based graphene sound source increases with the input power (Figure 2c). The linear fitting line shows that the output SP has the linear relation with the input power. The Rayleigh distance can be defined as $R_0 = A/\lambda_0$[23] with respect to sound source area A and isentropic sound wavelength λ_0. Figure 2d shows the SP emission from graphene *vs* the distance. For our thermophones tested at 16 kHz sound frequency, the Rayleigh distance is about 4.7 × 10^{-3} m. SP was tested at the distance of (1−10) × 10^{-2} m which belongs to the far-field. The fitting line illustrates that the output SP is inversely proportional to distance, which is in agreement with

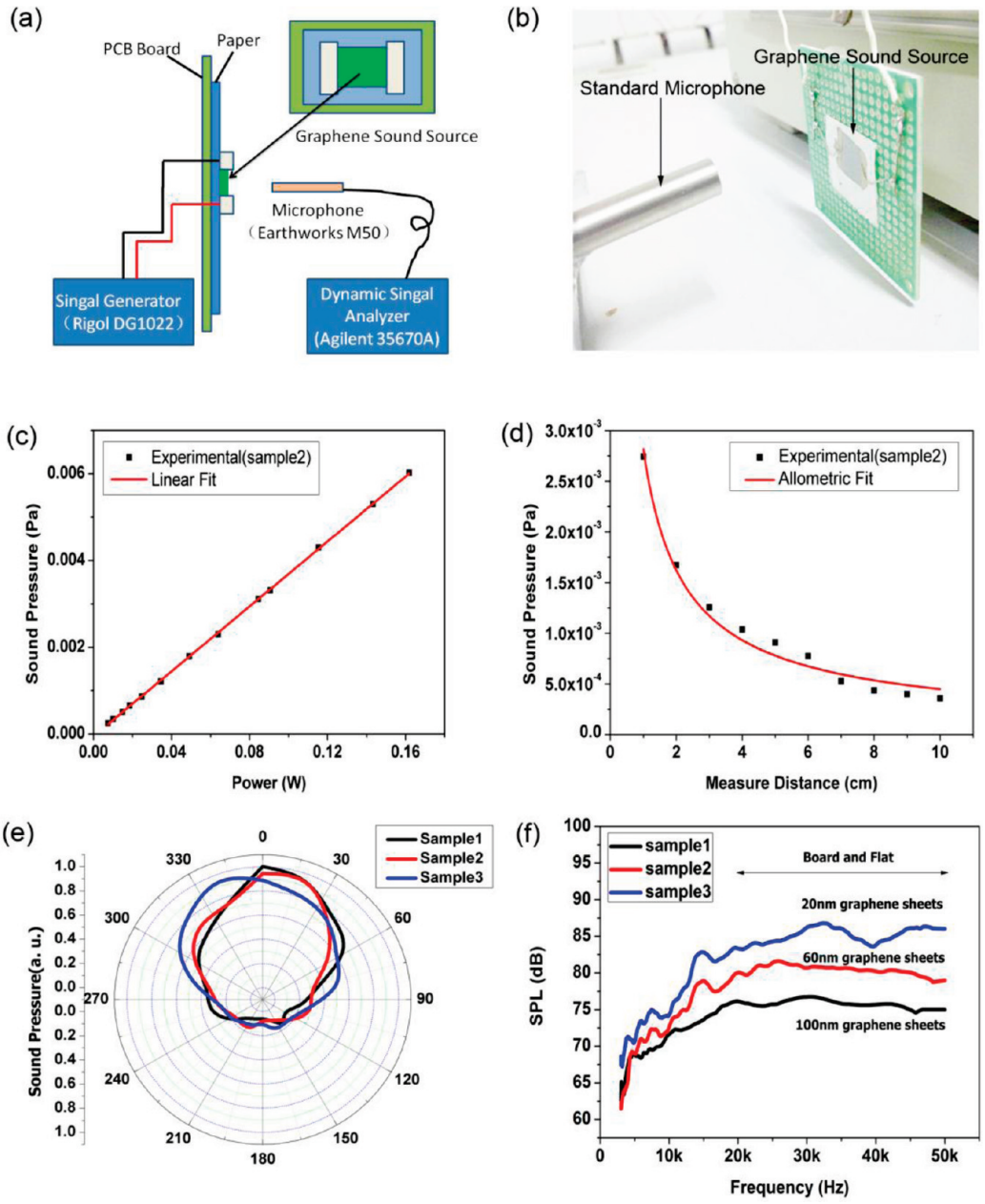

Figure 2. The acoustic test platform and test results of graphene sound source. (a) Schematic diagram of test platform. (b) On-site photo of the experimental setup. (c) The output SP from graphene *vs* the input power. The SP is recorded at conditions of 16 kHz sound frequency and 5 cm distance. (d) The plot of the output SP of graphene *vs* the measurement distance. The SP is recorded at 16 kHz sound frequency and 0.02 W input power. (e) Directivity of the graphene sound source in far-field. The three curves are in arbitrary SP units on-axis. The SP is recorded at 16 kHz sound frequency, 5 cm distance and 0.02 W input power. (f) The output sound pressure *vs* the frequency. The three curves are normalized with the input power 1 W/cm^2. The sound frequency is ranging from 3 to 50 kHz. The SP is recorded at the diatance of 5 cm and input power of 0.19, 0.07, and 0.01 W for three samples, respectively.

the estimate of far-field. When the measure distance is 5 cm at 16 kHz sound frequency, the omni-directional dispersion patterns can be achieved by testing the change of the SP with the receiving angle. The far-field directivity of the graphene sound source in Figure 2e shows that the main sound radiation area is near on-axis ±30 angles. The increase of angle leads to the decrease of SP in general. The relation between the output sound pressure level (SPL) and the frequency is shown in Figure 2f. The frequency is sweeping from 3 to 50 kHz. The three curves are normalized with the same power density (1 W/cm^2). The 20 nm graphene sound source ranks first in the SP performance due to its lowest HCPUA. The 60 nm and 100 nm graphene rank second and third, respectively. It indicates that thinner graphene sheets can produce higher SPL. The sound frequency band can cover audible and ultrasound. Especially in ultrasound range 20−50 kHz, there exists flat frequency response.

Different theoretical models for thermophones were compared. The carbon nanotube (CNT) loudspeaker

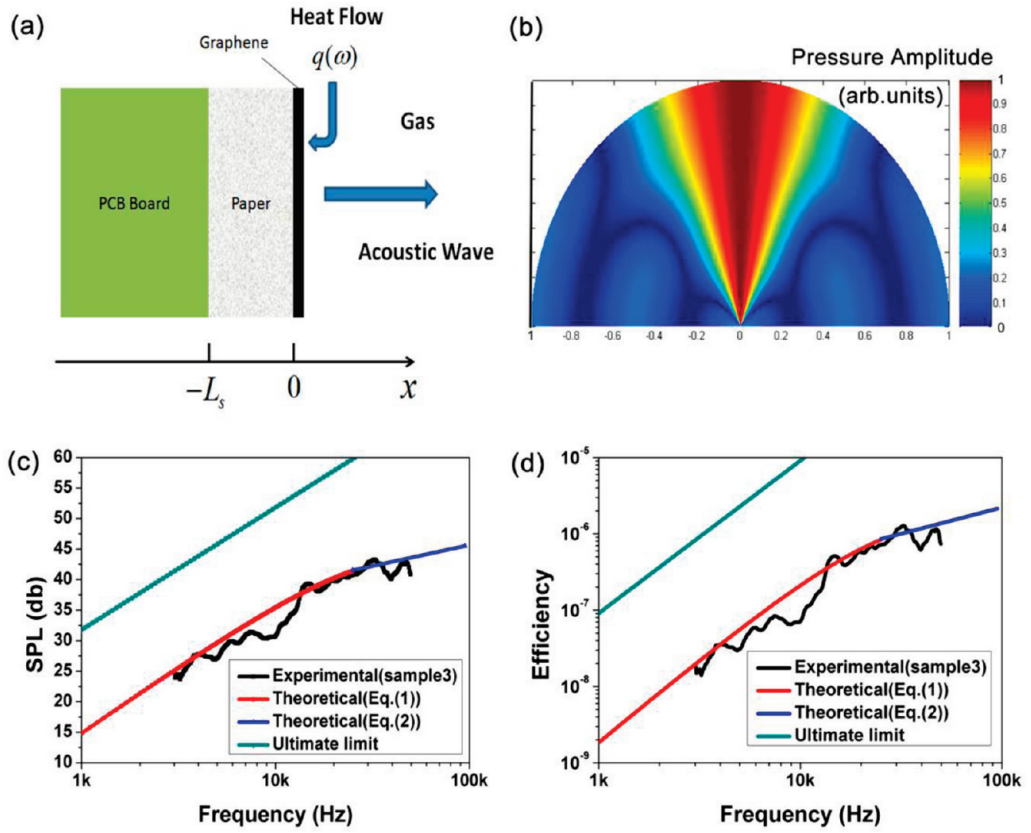

Figure 3. Theoretical model and results of graphene sound source. (a) Theoretical model of the graphene sound source. (b) Theoretical half-space directivity of the graphene sound source in far-field. (c) The theoretical and experimental results of SPL *vs* the frequency for sample 3. The SP is recorded at the distance of 5 cm and the input power of 0.01 W. (d) The theoretical and experimental results of efficiency *vs* frequency for sample 3.

which was made by Xiao *et al.*[19] radiated sound into full-space. However, graphene-on-paper device radiates sound into half-space. There exists the emission of thermal waves influenced by the heat-absorbing paper substrate. The thermally induced ultrasonic from porous silicon which was produced by Shinoda *et al.*[18] has a similar structure to graphene-on-paper. However, Shinoda's theory is not suitable for an on-substrate thermophone at low frequencies. On the basis of Shinoda's work, Hu *et al.*[24] put forward a model which can explain the thermophone both at low and high frequencies. Nevertheless, both of them omitted the 30 nm aluminum which functioned as the heat source in their models. They assumed that the conductor was thin enough that this part of impact could be neglected. In fact, their models are at the upper bound of the prediction of SP because the existence of the conductor's HCPUA, which can absorb heat. In our experiment, the thinner graphene shows a higher SP in Figure 2f, which can not be explained by those models, therefore the original model should be modified by considering the conductor's HCUPA. In addition, the equations of Hu *et al.* were derived in near-field. However, our experimental frequency response belongs to far-field. The equations can be simply transferred to far-field by multiplying R_0/r_0.[30]

For $f < \alpha_s/(4\pi L_s^2)$ at low frequencies in far-field, the SP can be written as

$$P_{rms} = \frac{R_0}{\sqrt{2}r_0}\frac{\gamma - 1}{v_g}\frac{e_g}{M(e_s + a_c) + e_g}q_0 \qquad (1)$$

For $f > \alpha_s/(4\pi L_s^2)$ at high frequencies in far-field, the SP can be written as

$$P_{rms} = \frac{R_0}{\sqrt{2}r_0}\frac{\gamma - 1}{v_g}\frac{e_g}{(e_s + a_c) + e_g}q_0 \qquad (2)$$

where f is frequency of sound; α_s and L_s is the thermal diffusivity and thickness of substrate, respectively; r_0 is the distance between sound source and the microphone; γ is the heat capacity ratio of gas; v_g is the sound velocity in gas; $e_i = (\kappa_i\rho_i C_{p,i})^{1/2}$ is the thermal effusivity of material i. The subscript i represent gas (g) or substrate (s), respectively. $a_c = (\kappa_c\rho_c C_s)^{1/2}$ is the thermal parameter of conductor (c); q_0 is the input power density; M is a frequency related factor (see Supporting Information). Under high frequency, $M \approx 1$, then eq 1 is the same as eq 2.

The modified formulas in near-field are also given (see Supporting Information eq 3 and 4). Comparing with the original formulas (see Supporting Information eq 1 and 2),[24] a factor $a_c = (\kappa_c\rho_c C_s)^{1/2}$ is introduced in our modified model, which takes into account the

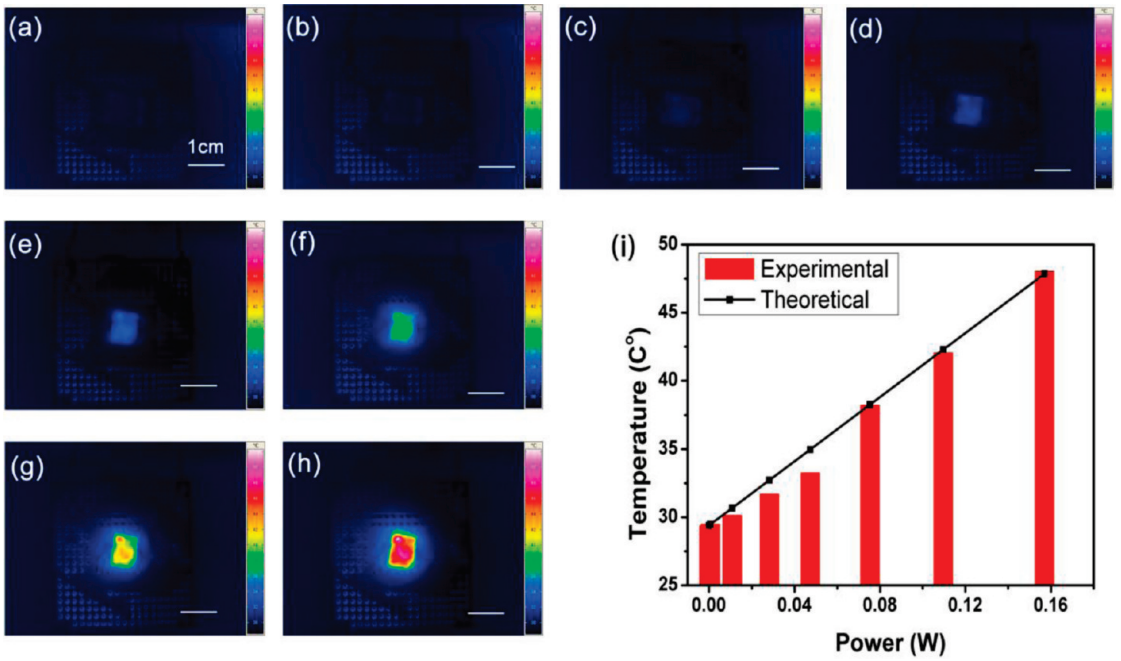

Figure 4. Infrared thermal images and average surface temperature of graphene (sample 2) with different amplitude of input power: (a) no power is applied; (b) input power q_o is 0.0007 W; (c) q_o is 0.01 W; (d) q_o is 0.03 W; (e) q_o is 0.05 W; (f) q_o is 0.08 W; (g) q_o is 0.11 W; (h) q_o is 0.16 W. (i) The average surface temperature of graphene *vs* the applied electric power. The experimental and theoretical results are shown. The SP is recorded at 16 kHz sound frequency and 5 cm measurement distance.

effect of the conductor. To demonstrate that this modified model is reasonable, the modified theoretical results are compared with the experimental results of Shinoda *et al.*[18] and the theoretical results of Hu *et al.*[24] (see Supporting Information Figure S6). Through comparison, our theoretical curve is slightly lower than that of Hu.[24] It indicates that the theoretical model of Hu *et al.*[24] is the upper bound SP. Our modified model considering the conductor's HCPUA is suitable with Shinoda's experimental results, so our modified model is applicable to graphene-on-paper structure.

The theoretical model for graphene-on-paper sound source device is shown in Figure 3a. Our model is a PCB board/paper/graphene/air multilayer structure. The sound emission component graphene has been considered. Considering the device as a point sound source in far-field, the theoretical half-space directivity $D(\theta,\varphi)$ is deduced by Vesterinen *et al.*[23]

$$D(\theta,\varphi) = \sin c\left(\frac{k_0 L_x}{2}\sin\theta\cos\varphi\right) \sin c\left(\frac{k_0 L_y}{2}\sin\theta\sin\varphi\right) \quad (3)$$

where the θ and φ are the angles of a spherical coordinate system; $k_0 = 2\pi/\lambda_0$ is the isentropic wavenumber. The sound source device is the origin of the system. L_X and L_y are sound source length and width, respectively.

Figure 3b shows the sound radiation of the graphene sound source in far-field. The on-axis direction has the largest sound intensity, the sound intensity decreases with the angle and the main intensity area

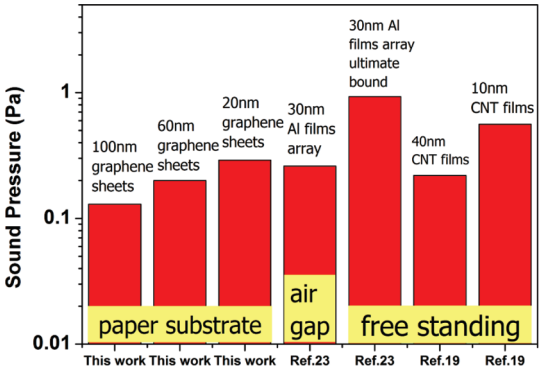

Figure 5. In far-field, comparison of sound pressure for a set of thermophones with the normalized values of 1 W input power, 5 cm measurement distance, and 20 kHz sound frequency. The substrates are also marked.

focuses on axis ±30° angles. Those results are accordance with the experimental directivity results in Figure 2e. Figure 3c shows the theoretical and experimental results of SPL *vs* the frequency for sample 3. The theoretical and experimental results are in good agreement. The small discrepancy could be explained by the surface roughness of the paper substrate.[23] The upper bound limit of SPL is also shown for comparison. The theoretical formula of the upper bound SP[23] is given by

$$P_{rms,max} = \frac{q_0 f}{\sqrt{2} r_0 C_{p,g} T_0} \quad (4)$$

where, $C_{p,g}$ is the specific heat of air; T_0 is ambient temperature.

TABLE 1. The Graphene Sound Source Performances Are Compared to Other Thermophones in Far-Field[a]

conductor	HCPUA (J/(m^2·K))	substrate	area (cm^2)	sound pressure (Pa)	reference
100 nm graphene sheets	1.5×10^{-1}	paper	1	0.13	this work
60 nm graphene sheets	9.3×10^{-2}	paper	1	0.20	this work
20 nm graphene sheets	3.1×10^{-2}	paper	1	0.29	this work
30 nm Al films array	7.3×10^{-2}	air gap	0.5	0.26	23
30 nm Al films array ultimate bound	7.3×10^{-2}	none (free standing)	0.5	0.93	23
40 nm CNT	3.1×10^{-2}	none (free standing)	9	0.22	19
10 nm CNT	7.7×10^{-3}	none (free standing)	9	0.56	19

[a] The values of input power and measurement distance are normalized with 1 W and 5 cm, respectively, and the sound frequency is 20 kHz.

On the basis of the spherical wave assumption, the efficiency of the graphene sound source can be calculated as $P_{rms}^2/(\rho_g v_g q_0)$.[23] Because of the interference effects at high frequency, the ultimate efficiency becomes saturation.[23] Figure 3d shows the efficiency of the graphene sound source. At the frequency of 32 kHz, sample 3 reaches its maximal efficiency. The upper bound efficiency line is also shown for reference. It is noted that the efficiency of our device is 1 order of magnitude lower than the ultimate bound. The SPL and efficiency analyses of the other two samples are also available in Supporting Information (Figures S7 and S8).

Arnold and Crandall[17] described the scene: While the thermophone was working, the electric power was converted into joule heating through conductor. It would heat up the air near its surface and then the sound pressure was generated by the changing of the air temperature. To demonstrate this phenomenon by experiments, advanced infrared thermal imaging instrumentation was used, which can measure the relations between the surface temperature distribution of graphene and the amplitude of input power. The electric power q_0 increases from 0 to 0.16 W gradually (Figure 4a−h). At each power stage, a picture is recorded until the surface temperature reaches a steady state. This means that the surface temperature is recorded at constant input power. The surface temperatures at different power stage (Figure 4a−h) are summarized (shown in Figure 4i (red pillars)). The average surface temperature of graphene increases when q_0 increases from 0 to 0.16 W gradually. The improvement of input power leads to the increase of surface temperature. The average surface temperature $\bar{T}$ can be predicted by a theoretical formula:[18]

$$\bar{T} = T_0 + \frac{q_o}{\sqrt{j\omega\kappa_s C_{p,s}}} \quad (5)$$

where κ_s and $C_{p,s}$ are the thermal conductivity and heat capacity of the paper substrate, respectively; ω is the angular frequency of sound.

The theoretical results of surface temperature are plotted in Figure 5i (black point and line). Results from calculation and experiments are in good agreement. From the test results as shown in Figure 2c, it reveals that the SP increases with the input power. Therefore, the surface temperature of graphene increases with the SP. It suggests that Joule heating has great relations with the intensity of sound. This also indicates that the working principle is related to thermoacoustic effect.

Figure 5 illustrates the comparison the sound performance among a set of thermophones in far-field. Table 1 lists those parameters in detail. According to the comparison, it is found that HCPUA of the conductor and the thermal properties of the substrate play important roles in the performance of thermophones. The HCPUA is relative to the conductor's type and its thickness. For the same kind of material, the thinner the films are, the higher the SPL becomes. A comparison with different kinds of substrates reveals that heat insulation materials can reduce heat leakage from the substrates. Free standing is an ideal and effective way to realize high SPL and efficiency. Paper is a good choice when a substrate is needed. We also compare the graphene and Al films[18] in near-field (see Supporting Information Tables S1 and S2). The graphene has higher SP than 30 nm Al due to the contribution of the paper substrate.

CONCLUSIONS

We demonstrated that graphene can emit sound which can expand its application in the acoustic field. Sound emission from graphene is measured as a function of power, distance, angle, and frequency in far-field. From 3 to 20 kHz, the SPL shows a linear relationship with frequency. In addition, significant broad and flat SPLs are obtained in the ultrasonic region, ranging from 20 to 50 kHz. A modified model has been established considering the impact of the conductor to analyze the sound frequency spectrum. Sound frequency is independent with sound response at high frequencies in near-field. In far-field, measured sound pressure and efficiency are in good agreement with theoretical results. The infrared thermal imaging of graphene indicates that the thermoacoustic effect is the working principle. The surface temperature of graphene increases with the input power which is in accordance with theoretical analysis. The performance of graphene sound source is compared to other thermophones both in far-field and near-field. It reveals

that the performance of thermophone mainly depends on the HCPUA of the conductor and the thermal properties of the substrate. The paper-based graphene sound source can be widely used because of its highly reliable, flexible, transparent, no vibration, simple structure and high quality characteristics. It can be made into speakers, buzzers, earphones, and ultrasonic detection and imaging, *etc.* Especially, it is very promising in multimedia, consumer electronics, biological, medical, and many other areas.

METHODS

Large-scale MLG films could be synthesized by using chemical vapor deposition.[31−38] To obtain the desired thickness of graphene films, OPE treatment (Supporting Information, Figure S1) was used.

Structure characteristics of the multilayered graphene films were analyzed from Raman spectrum obtained by Raman spectroscopy with a Renishaw R-1000 system using wavelength of 514.5 nm. The surface morphology was observed by SEM (DI-3100). The thickness and surface roughness of the films were measured using a surface profiler (Dektak150, Veeko). Sheet resistance was measured by the automatic four point probe meter (model 280SI, Four Dimensions, Inc.). The interlayer distance of multilayered graphene was measured (Supporting Information, Figure S2) by the X-ray diffractometer (XRD, Rigaku).

We fabricated paper substrates by cutting filter paper (30−50 um hole, BB90-DXLZ) using a laser cutter (Figure 1a). We manually transferred the graphene on the paper (Supporting Information, Figure S3), and contacted pads using low-resistivity sliver ink. A stencil mask was generated by cutting designed patterns using a laser cutter, then we placed the stencil mask on top of the patterned paper, and filled the openings of the stencil mask with silver ink. The paper was then attached to PCB board which was used to improve the mechanical strength and establish electrical connection. The paper device was baked at 80 °C for 10 min.

The acoustic platform for testing the graphene sound source contains a signal generator, a standard microphone, and a dynamic signal analyzer. The $^1/_4$ in. standard microphone (Earthworks M50), which had a very flat frequency response reaching up to 50 kHz and a 31 mV/Pa high sensitivity, was used to measure the SPL of the graphene sound source. The signal analyzer (Agilent 35670A) was used to make fast Fourier transform analysis and record the value of SPL. Our test results were measured in a soundproof box. The box size was $1 \times 0.5 \times 0.5\ m^3$. To avoid the effects of reflections, the box was filled with sound-absorbing sponges.

Acknowledgment. Thanks for the support from G. Zhang, Z.W. Liu, L. Harri, and H.W. Zhu. This work is supported by the National Natural Science Foundation (61025021, 60936002, 60729308, 51072089, 61011130296, and 61020106006), National Key Project of Science and Technology (2009ZX02023-001-3), National 863 Project (2006AA04Z372), and International Cooperation Project from Ministry of Science and Technology (2008DFA12000) of China.

Supporting Information Available: Description of the preparation, measurement, and theoretical analysis for the graphene sound source and three videos. This material is available free of charge *via* the Internet at http://pubs.acs.org.

REFERENCES AND NOTES

1. Novoselov, K. S.; Geim, A. K.; Morozov, S. V.; Jiang, D.; Zhang, Y.; Dubonos, S. V.; Grigorieva, I. V.; Firsov, A. A. Electric Field Effect in Atomically Thin Carbon Films. *Science* **2004**, *306*, 666–669.
2. Geim, A. K.; Novoselov, K. S. The Rise of Graphene. *Nat. Mater.* **2007**, *6*, 183–191.
3. Geim, A. K. Graphene: Status and Prospects. *Science* **2009**, *324*, 1530–1534.
4. Balandin, A. A.; Ghosh, S.; Bao, W. Z.; Calizo, I.; Teweldebrhan, D.; Miao, F.; Lau, C. N. Superior Thermal Conductivity of Single-Layer Graphene. *Nano Lett.* **2008**, *8*, 902–907.
5. Lin, Y. M.; Dimitrakopoulos, C.; Jenkins, K. A.; Farmer, D. B.; Chiu, H. Y.; Grill, A.; Avouris, Ph. 100-Ghz Transistors from Wafer-Scale Epitaxial Graphene. *Science* **2010**, *327*, 662.
6. Zheng, Y.; Ni, G. X.; Toh, C. T.; Zeng, M. G.; Chen, S. T.; Yao, K.; Özyilmaz, B. Gate-Controlled Nonvolatile Graphene-Ferroelectric Memory. *Appl. Phys. Lett.* **2009**, *94*, 163505.
7. Bunch, J. S.; Zande, A. M.; Verbridge, S. S.; Frank, I. W.; Tanenbaum, D. M.; Parpia, J. M.; Craighead, H. G.; McEuen, P. L. Electromechanical Resonators from Graphene Sheets. *Science* **2007**, *315*, 490–493.
8. Li, X. S.; Zhu, Y. W.; Cai, W. W.; Borysiak, M.; Han, B. Y.; Chen, D.; Piner, R. D.; Colombo, L.; Ruoff, R. S. Transfer of Large-Area Graphene Films for High-Performance Transparent Conductive Electrodes. *Nano Lett* **2009**, *9*, 4359–4363.
9. Xia, F. N.; Mueller, T.; Lin, Y. M.; Garcia, A. V.; Avouris, P. Ultrafast Graphene Photodetector. *Nat. Nanotechnol* **2009**, *4*, 839–843.
10. Schedin, F.; Geim, A. K.; Morozov, S. V.; Hill, E. W.; Blake, P.; Katsnelson, M. I.; Novoselov, K. S. Detection of Individual Gas Molecules Adsorbed on Graphene. *Nat. Mater.* **2007**, *6*, 652–655.
11. Ghosh, S.; Calizo, I.; Teweldebrhan, D.; Pokatilov, E. P.; Nika, D. L.; Balandin, A. A.; Bao, W.; Miao, F.; Lau, C. N. Extremely High Thermal Conductivity of Graphene: Prospects for Thermal Management Applications in Nanoelectronic Circuits. *Appl. Phys. Lett.* **2008**, *92*, 151911.
12. Jae, H. S.; Insun, J.; Arden, L. M.; Lucas, L.; Zachary, H. A.; Michael, T. P.; Li, X. S.; Yao, Z.; Huang, R.; Broido, D.; *et al.* Two-Dimensional Phonon Transport in Supported Graphene. *Science* **2010**, *328*, 213–216.
13. Prasher, R. Graphene Spreads the Heat. *Science* **2010**, *328*, 185–186.
14. Dungchai, W.; Chailapakul, O.; Henry, C. S. Electrochemical Detection for Paper-Based Microfluidics. *Anal. Chem.* **2009**, *81*, 5821–5826.
15. Martinez, A. W.; Phillips, S. T.; Whitesides, G. M.; Carrilho, E. Diagnostics for the Developing World: Microfluidic Paper-Based Analytical Devices. *Anal. Chem.* **2010**, *82*, 3–10.
16. Liu, X. Y.; Brien, M. O.; Mwangi, M.; Whitesides, G. M.; Li, X. J. Paper-Based Piezoresistive MEMS Force Sensors. *IEEE 24th Int. Conf. MEMS* **2011**, 133–136.
17. Arnold, H. D.; Crandall, I. B. The Thermophone as a Precision Source of Sound. *Phys. Rev.* **1917**, *10*, 22–38.
18. Shinoda, H.; Nakajima, T.; Ueno, K.; Koshida., N. Thermally Induced Ultrasonic Emission from Porous Silicon. *Nature* **1999**, *400*, 853–855.
19. Xiao, L.; Chen, Z.; Feng, C.; Liu, L.; Bai, Z. Q.; Wang, Y.; Qian, L.; Zhang, Y. Y.; Li, Q. Q.; Jiang, K. L. Flexible, Stretchable, Transparent Carbon Nanotube Thin Film Loudspeakers. *Nano Lett.* **2008**, *8*, 4539–4545.
20. Niskanen, A. O.; Hassel, J.; Tikander, M.; Maijala, P.; Grönberg, L.; Helistö, P. Suspended Metal Wire Array as a Thermoacoustic Sound Source. *Appl. Phys. Lett.* **2009**, *95*, 163102.
21. Kozlov, M. E.; Haines, C. S.; Oh, J.; Lima, M. D.; Fang, S. L. Sound of Carbon Nanotube Assemblies. *J. Appl. Phys.* **2009**, *106*, 124311.

22. Aliev, A. E.; Lima, M. D.; Fang, S. l.; Baughman, R. H. Underwater Sound Generation Using Carbon Nanotube Projectors. *Nano Lett.* **2010**, *10*, 2374–2380.
23. Vesterinen, V.; Niskanen, A. O.; Hassel, J.; Helisto, P. Fundamental Efficiency of Nanothermophones: Modeling and Experiments. *Nano Lett.* **2010**, *10*, 5020–5024.
24. Hu, H.; Zhu, T.; Xu, J. Model for Thermoacoustic Emission from Solids. *Appl. Phys. Lett.* **2010**, *96*, 214101.
25. Venkatasubramanian, R. Nanothermal Trumpets. *Nature* **2010**, *463*, 619.
26. Niskanen, A.; Hassel, J.; Helistoe, P. Sound Source Using Conductor Thermally Decoupled in the Middle Part from Substrate Based on the Thermoacoustic Effect. *PCT Int. Appl.* 2010, WO 2010061060 A1 20100603.
27. Suzuki, K.; Sakakibara, S.; Okada, M.; Neo, Y.; Mimura, H.; Inoue, Y.; Murata, T. Study of Carbon-Nanotube Web Thermoacoustic Loud Speakers. *Jpn. J. Appl. Phys.* **2011**, *50*, 01BJ10.
28. Dervishi, E.; Li, Z. R.; Watanabe, F.; Courte, A.; Biswas, A.; Biris, A. R.; Saini, V.; Xu, Y.; Biris, A. S. Versatile Catalytic System for the Large-Scale and Controlled Synthesis of Single-Wall, Double-Wall, Multi-Wall, and Graphene Carbon Nanostructures. *Chem. Mater.* **2009**, *21*, 5491–5498.
29. Wang, D. W.; Li, F.; Wu, Z. S.; Ren, W. C.; Cheng, H. M. Electrochemical Interfacial Capacitance in Multilayer Graphene Sheets: Dependence on Number of Stacking Layers. *Electrochem. Commun.* **2009**, *11*, 1729–1732.
30. Blackstock, D. T. *Fundamentals of Physical Acoustics*; John Wiley and Sons, Ltd: New York, 2000; pp 440—465.
31. Kim, K. S.; Zhao, Y.; Jang, H.; Lee, S. Y.; Kim, J. M.; Kim, K. S.; Ahn, J. H.; Kim, P.; Choi, J. Y.; Hong, B. H. Large-Scale Pattern Growth of Graphene Films for Stretchable Transparent Electrodes. *Nature* **2009**, *457*, 706–710.
32. Li, X. S.; Cai, W. W.; An, J.; Kim, S.; Nah, J.; Yang, D. X.; Piner, R.; Velamakanni, A.; Jung, I.; Tutuc, E.; *et al*. Large-Area Synthesis of High-Quality and Uniform Graphene Films on Copper Foils. *Science* **2009**, *324*, 1312–1314.
33. Lee, Y. H.; Lee, J. H. Catalyst Patterned Growth of Interconnecting Graphene Layer on SiO_2/Si Substrate for Integrated Devices. *Appl. Phys. Lett.* **2009**, *95*, 143102.
34. Reina, A.; Jia, X. T.; Ho, J.; Nezich, D.; Son, H.; Bulovic, V.; Dresselhaus, M. S.; Kong, J. Few-Layer Graphene Films on Arbitrary Substrates by Chemical Vapor Deposition. *Nano Lett.* **2009**, *9*, 30–35.
35. Robinson, J. A.; Puls, C. P.; Staley, N. E.; Stitt, J. P.; Fanton, M. A.; Emtsev, K. V.; Seyller, T.; Liu, Y. Raman Topography and Strain Uniformity of Large-Area Epitaxial Graphene. *Nano Lett.* **2009**, *9*, 964–968.
36. Lee, Y. H.; Lee, J. H. Scalable Growth of Free-Standing Graphene Wafers with Copper(Cu) Catalyst on SiO_2 /Si Substrate: Thermal Conductivity of the Wafers. *Appl. Phy. Lett.* **2010**, *96*, 083101.
37. Lee, Y.; Bae, S.; Jang, H.; Jang, S.; Zhu, S. E.; Sim, S. H.; Song, Y. I.; Hong, B. H.; Ahn, J. H. Wafer-Scale Synthesis and Transfer of Graphene Films. *Nano Lett.* **2010**, *10*, 490–493.
38. Li, X. M.; Zhu, H. W.; Wang, K. L.; Cao, A, Y.; Wei, J. Q.; Li, C. Y.; Jia, Y.; Li, Z.; Li, X.; Wu, D. H. Graphene-on-Silicon Schottky Junction Solar Cells. *Adv. Mater.* **2010**, *22*, 2743–2748.